Journal of Manufacturing Processes 109 (2024) 222–234

Contents lists available at ScienceDirect

Journal of Manufacturing Processes

journal homepage: www.elsevier.com/locate/manpro

Advanced process characterization and machine learning-based correlations between interdiffusion layer and expulsion in spot welding

Joseph Kershaw [a], Hassan Ghassemi-Armaki [c], Blair E. Carlson [c], Peng Wang [a,b,*]

[a] Department of Mechanical Engineering, University of Kentucky, 151 Ralph G. Anderson Building, Lexington, KY 40506, USA
[b] Department of Electrical and Computer Engineering, University of Kentucky, 351 Ralph G. Anderson Building, Lexington, KY 40506, USA
[c] Global Research and Development, General Motors, 30470 Harley Earl Blvd, Warren, MI 48092, USA

ARTICLE INFO

Keywords:
Resistance spot welding
Process modeling
Quality prediction
Defect detection
Neural networks

ABSTRACT

Over the past decades, substantial endeavors have been dedicated to unraveling the intricacies inherent to Resistance Spot Welding (RSW). However, a comprehensive and consensual understanding of the RSW process physics is still lacking, including the exact number of physical phases behind the RSW process. For example, a widely accepted model indicates that metal only starts melting after the peak of dynamic resistance, while the latest research on welding uncoated materials challenges this by suggesting that melting begins around the resistance peak. Furthermore, most of existing physical models only consider welding materials without coatings in a controlled lab setting, whereas coated sheet metal is the norm in real production. Addressing these challenges, this paper introduces an enhanced model for RSW that considers the melting phase of the coating's InterDiffusion Layer (IDL) in Press Hardening Steels (PHS). This phase is believed to influence both welding quality and the occurrence of expulsions. Additionally, the timing at which each phase starts has been determined by analyzing real-time, multi-variable sensing data from various welding scenarios, and a signal processing technique has been devised to automatically identify when these phases begin. Leveraging this refined process understanding and characterization, meaningful explainable features are extracted, and a data-driven multilayer perceptron model is constructed for 1) predicting IDL thickness and 2) detecting expulsions upon predicted IDL thickness. The experimental results validate that the proposed IDL-inclusive model advances existing physical models for RSW and the IDL prediction improves the RSW defect detection and process monitoring.

1. Introduction

RSW stands as a widely employed technique for joining, involving the permanent fusion of two or more pieces of sheet metal. This technique, renowned as one of the oldest and most prevalent autonomous manufacturing processes globally, finds its principal application primarily in the automotive and aerospace sectors [1]. The RSW process creates a permanent bond by clamping a sheet metal stack-up between two electrodes. Through the passage of an electric current, the sheet metal functions as a resistor within an electrical circuit, leading to localized heating and subsequent liquefaction of the metal at the point of contact with the electrodes. Once the current is stopped, the liquid metal cools and solidifies, effectively creating a region of continuous metal known as a nugget [2]. This nugget acts as a permanent fastener, akin to a rivet, but requires no additional components or preprocessing and adds no additional weight.

In comparison to traditional fastening methods, RSW faces a drawback in terms of consistency. RSW involves a complex interplay of electrical, mechanical, thermal, and fluid mechanics, which are all suspectable to process and material variations. Alongside the common challenges encountered in other manufacturing processes, such as tool wear and material fit-up conditions, minor changes in the chemical composition and microstructure of metal sheets can wield huge impacts on the final nugget quality [3]. The intricacies and variability intrinsic to RSW lead to predicaments both in process planning and execution in a real production line. Whenever manufacturers want to introduce even a slightly altered welding condition compared to previously used ones, a new set of process parameters would need to be formulated through trial and error to attain the desired welding quality [4]. Furthermore, these parameters are designed to optimize the likelihood of a successful weld,

* Corresponding author. at: Department of Mechanical Engineering, University of Kentucky, 151 Ralph G. Anderson Building, Lexington, KY 40506, USA.
E-mail address: edward.wang@uky.edu (P. Wang).

https://doi.org/10.1016/j.jmapro.2023.12.013
Received 1 September 2023; Received in revised form 27 October 2023; Accepted 7 December 2023
Available online 19 December 2023

without guaranteeing it. The inherent process variability leads to uncertainties in the final integrity of the nugget. Crucially, two primary defects can manifest within a weld, and they prove difficult, if not feasible, to be detected upon visual inspection. The first is an underdeveloped weld nugget, resulting in a bonded stack-up lacking the strength characteristic of a desired weld. The second is expulsion, wherein molten metal is suddenly expelled away from the weld nugget, leading to abnormal geometry and reduced nugget volume. Conventional means of identifying these defects involve either destructive testing or expensive ultrasonic sensing [5]. To enhance both process refinement and quality assurance, substantial endeavors have been dedicated to unraveling the intricacies inherent to the RSW process, leading to continuously improved process characterization and modeling.

One of the most significant contributions to monitoring and elucidating the RSW process was undertaken by Dickenson in the 1980s [6]. This model observed the time series data of the Dynamic Resistance (DR) and correspondingly linked the shifting trends in the data to discrete phases of the welding process. Each phase was subsequentially associated with a physical phenomenon capable of accounting for the observed changes. Researchers further investigated this model and Dickenson's postulations through more advanced process sensing and more comprehensive experimental studies. For example, experiments using electrode displacement sensors unveiled that the material dimensional changes exerted a more pronounced influence on the DR trends than previously assumed [7]. Over time, efforts have been made to extend the model's applicability, for instance concerning coated materials. Models developed with coated materials unveiled the existence of additional phases arising due to the incorporation of coatings [8]. Despite a broadly accurate depiction of the process physics by these models, there are still ongoing debates about when the individual physical phase starts. For example, the Dickenson model asserted that the metal begins melting strictly after the peak of the DR, which encountered considerable debate. The latest study on uncoated material welding indicates that melting occurs *around* the DR peak, while largely maintaining consistency with the remaining aspects of the traditional model [9]. Nonetheless, the state-of-the-art RSW models have two limitations when considering their applicability for integration into a production line. Firstly, these models have not been generalized to coated materials that predominate modern manufacturing practices, more specifically the specific phenomena and timing of the IDL-related phase. Secondly, most models heavily rely on human subjective knowledge or experiential insights to determine the initiation timing of distinct process phases, and an automated methodology for segregating these phases is conspicuously absent. One solution to the second challenge involves the utilization of advanced process sensing and characterization techniques. With an abundant dataset of process sensing information encompassing diverse welding scenarios, it becomes possible to analyze big data in a cluster to uncover overarching patterns associated with common phases shared in the diverse welding conditions and transitions between subsequent phases.

Manufacturing process monitoring is a critical aspect of "Industry 4.0", and it is often accompanied by advanced data analytics algorithms to aid in real-time decision making, e.g., defect detection, quality prediction, and process planning [10]. One of the main roadblocks to the widespread adoption of this new paradigm is the required investment. Alongside procuring and integrating the essential sensors into the machinery, the essential IT and OT requisites for aggregating data into decision-making pipeline also present a considerable challenge [11]. Fortunately, many existing RSW production lines have already implemented sensing technology and data storage/analytics platforms for general in-line process monitoring. As a result, a substantial portion of the initial capital investment has already been deployed, although vast amounts of welding data remain underutilized within server facilities. This renders RSW an advantageous entry point for manufacturers to transition toward the pipeline of Industry 4.0, improved decision making and quality assurance upon process sensing. The most prevalent type of process sensing in RSW is DR, due to its acute sensitivity to perturbations occurring during the welding process. It effectively reflects the thermal and electrical dynamics [12]. Additionally, capturing the mechanical and fluid dynamics, such as thermal strain and deformation, can be inferred through the sensing of welding force and electrode displacement [7].

Most physical RSW models provide qualitative understanding of the underlying phenomena, i.e., uncovering complicated physical activities during individual phases. These models are less capable of quantitative welding quality prediction, e.g., nugget size prediction and expulsion defect detection. Upon process sensing, Machine Learning (ML) techniques are very promising at quantitative process modeling and predictive analysis. In general, there are two types of ML techniques for RSW process modeling and quality prediction: advanced ML models that can directly correlate raw sensing data into quality/defects; and standard ML models that rely on feature extraction from process sensing. Related to the first approach, recurrent neural networks have been investigated to predict the Heat Affected Zone (HAZ) from the DR and welding power [13], an adaptive resonance theory neural network has been developed to predict the nugget size, strength, and failure mode upon voltage and current time series [14], and 1-D convolutional neural networks have been studied to correlate nugget formation metrics from the time series of the current, DR, Force, and Displacement [15]. The challenge associated with this approach is that the rationale behind how the algorithm arrives at its conclusions lacks transparency or explainability. Manufacturers are typically hesitant to embrace control algorithms that lack a clear and logical rationale for their production line operations [16]. The second ML approach, using pre-defined features related to identified physical phases as modeling inputs, is more explainable. For example, DR features such as peaks have been used by a neuro-fuzzy interface model for the prediction of weld strength [17], random forest model to classify cold, expulsed, or acceptable welds [19], and support vector regression for quality prediction [18]. More advanced features, such as frequency-domain features and advanced statistical features (e.g., skewness and kurtosis), have also been studied for detecting sheet misalignments [20], predicting nugget size [21], and detecting electrode wear [22]. However, the effectiveness of this ML approach is greatly contingent on the inclusivity and thoroughness of the features used, which are typically pre-defined upon physical comprehension of the underlying process phenomena and characteristics. Consequently, an enhanced understanding of the intricacies of the Resistance Spot Welding (RSW) process translates to the acquisition of more comprehensive and meaningful features. This, in turn, contributes to bolstering the reliability and precision of process monitoring, defect detection, and the evaluation of welding quality.

The contribution of this paper lies in three folds:

1) An enhanced RSW model is introduced to consider the melting and removal of the coating's IDL in PHS, which is hypothesized to influence both welding quality and the occurrence of expulsions. The suggested 4 phases of the RSW process are defined as material expansion, IDL removal, pre-molten joining, and nugget formation.
2) Key phase transition points have been determined by analyzing multi-variable sensing data from various welding scenarios, and a systematic method that combines data filtering, topographic prominence, and logical rules has been developed to automatically identify when the suggested 4 phases begin.
3) Leveraging this refined process characterization, meaningful explainable features are extracted from process sensing data, and a data-driven multilayer perceptron model is constructed for correlating the extracted features to predicting IDL thickness and detecting expulsions.

The following sections cover the development of each of these goals, starting with a review of existing physical models and introducing the advanced RSW model in Section 2. This is followed by the development

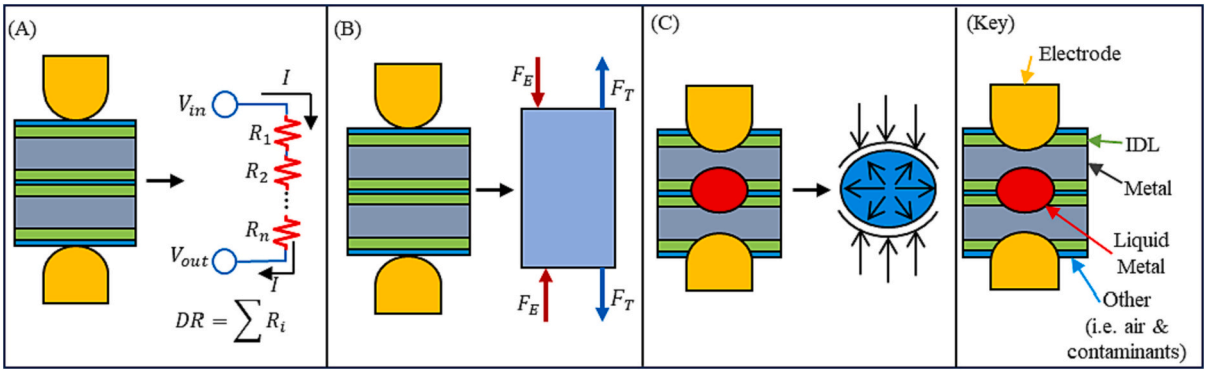

Fig. 1. Illustration of physical mechanisms involved in RSW: (A) equivalent circuit diagram, (B) static model, (C) pressure diagram, and (Key) key to colors used in welding illustrations.

of the methodologies required to automatically segregate these phases and extract the features from the process monitoring data in Section 3. This finally leads to the development of a multilayer perceptron for correlating features to IDL thickness prediction and exposition detection in Section 4 and experimental studies in Sections 5 and 6.

2. Advanced process characterization and physical models

The section starts with an overview of the fundamental physics that underpin RSW, as well as presenting an overview of the most current physical models, along with their capabilities and constraints. Subsequently, a particular area often overlooked in prevailing models, the coating and IDL in sheet metal and its consequential effect on expulsions, is then discussed. Following this, the proposed model for RSW, encompassing the IDL and comprising four distinctive phases, is explained, specifically on the underlying physical mechanisms characterizing each of these phases.

2.1. Present RSW models

RSW involves a complex interplay of electrical resistance, solid mechanics, and fluid dynamics. Explanatory models incorporating concepts within each of these fields to form a complete picture. From an electrical perspective, the RSW process can be conceptualized as a basic circuit configuration, encompassing a voltage source and a sink, represented by the two electrodes. These electrodes are separated by a series of resistive elements in a stack-up, which include the metal, coating, IDL, and any contaminants, that can be combined together to form the total DR, shown on Fig. 1A. The resistance of each element is correlated by the material thickness and resistivity [23]. During welding, the thickness will gen will generally first expand and then contract throughout the process, while the resistivity of material increases as temperature increases [24].

From the solid mechanics perspective, two primary forces are involved in the process, the electrode clamping force and thermal expansion force, as shown in Fig. 1B. Thermal expansion is the root cause of the gradually increasing displacement between electrodes and electrode force [25]. Both these elements increase with temperature, while the modulus of elasticity has noticeable decreases when the metal approaches the melting point, decreasing the expansion force [26,27]. After liquification, the process is governed by fluid dynamics. Given the ongoing rise in temperature, the molten pool tries to expand in all directions, yet it favors the path of the least resistance, as depicted in Fig. 1C. As a result, the metal undergoes radial expansion in addition to axial expansion, effectively diverting a portion of the force and material away from the applied load [28].

The most prevalent and well-established model was proposed by Dickenson et al. in the 1980's [6]. Their analysis predominantly focused on the DR change throughout the welding process, and led to the proposition of five distinct stages, as shown in the left part of Fig. 2. The first phase involves a breakdown of external contaminants that act as resistive material within the process. The second phase corresponds to material softening and compression, minimizing small gaps between sheet metals and increasing contact area between electrodes and stack-up. The third phase is characterized by an elevation in DR, caused by the temperature rises in the bulk material. In the fourth phase, material liquefaction initiates, further augmenting the contact area for current conduction. Simultaneously, the sheet metal reaches a softened state, reducing the distance between two electrodes under the applied electrode force. The increasing contact area and decreasing electrode

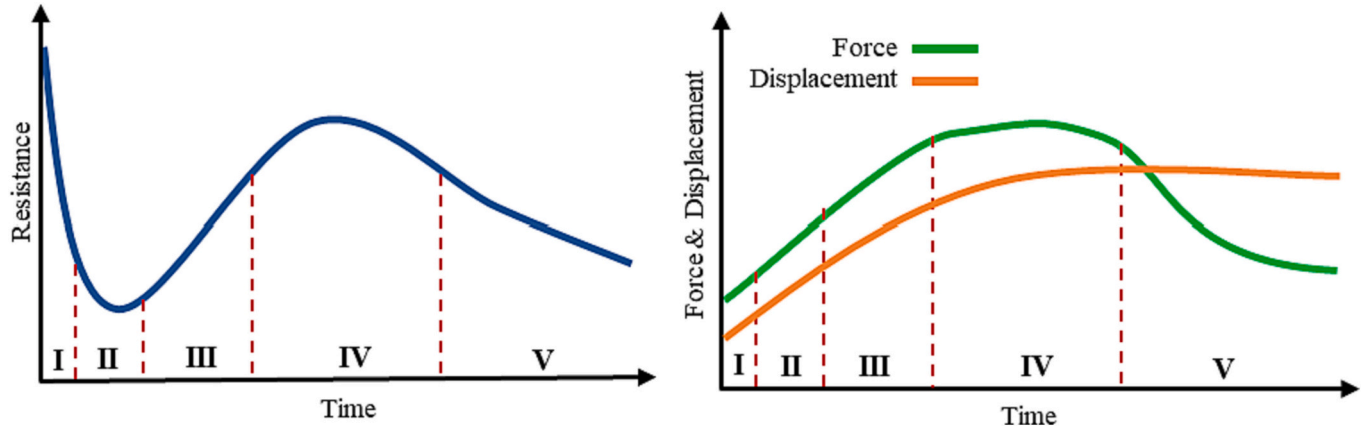

Fig. 2. 5-Phase Dickenson model: (left) DR curve, (right) force and displacement curves.

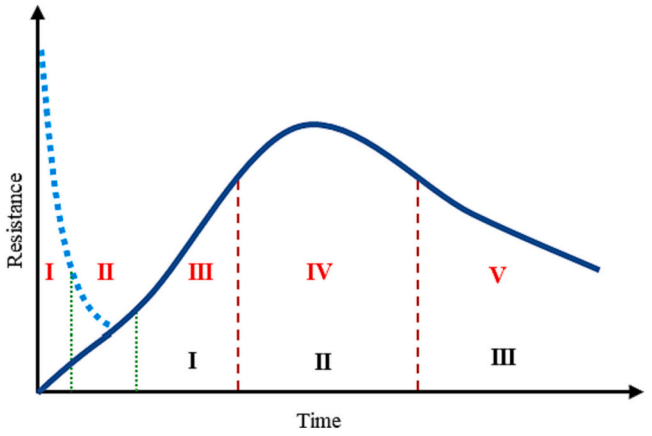

Fig. 3. Transformer DR curves (solid curve) vs. Sensor DR curves (dashed curve). Original phase numbers of the Dickinson model shown in red vs. phase numbers of the referenced 3-phase model shown in black. (For interpretation of the references to color in this figure legend, the reader is referred to the web version of this article.)

distance together reverse the increasing DR. The last phase is a continuation of the downward trend, as the metal achieves full liquification and the ultimate molten region forms toward the nugget.

Additional models based on the analysis of mechanical measurements, i.e., electrode force and displacement, have been able to provide additional insight into the process. As can be seen in the right part of Fig. 2, the force and displacement exhibit a consistent upward trajectory through the majority of the process, reaching equilibrium and subsequently declining during the liquification stage. This observation underscores that the increase in resistance during early phases stems from the thermal expansion of the material, while also confirming that plastic deformation is a cause of the lowering resistance in later phases [7]. The foundational concept of Dickenson model is robust, and the phases preceding liquification have been thoroughly investigated and validated [12]. However, it is important to note that this model is not fully perfect, and there are some ongoing discussions regarding the precise timing of liquification and the onset of nugget formation. Recent models have suggested that the nugget formation can occur at any point during phase 4, rather than being strictly limited to strictly after the DR peak [9].

Despite advancements in understanding the RSW process, the derived features derived from these models are still limited in scope. These features primarily center on the peak DR during phase 4 and the difference between the peak and concluding resistance. Furthermore, these models confront two issues that prevent their application in production. Firstly, these models have not been generalized to coated materials that predominate modern manufacturing practices. Secondly, most of these works leverage lab-grade setups and directly measure the DR through auxiliary sensors, e.g., Hall-Effect device or Rogowski coils. In contrast, industrial RSW systems gauge the current through a secondary transformer, which renders the initial DR drop imperceptible (see Fig. 3). This turns the original 5-Phase model to a 3-Phase model: *Thermal Expansion*, *Initial Liquification*, and *Nugget Formation*. Since this paper originated from RSW plant data analysis, for clarity, the rest of the paper will refer to the Dickinson model as the 3-Phase model, with the first phase corresponding to thermal expansion.

2.2. Metal coating and Interdiffusion layer for press hardening steels

As stated previously, most existing models primarily focus on uncoated sheet metals due to the introduction of an additional variable that proves challenging to control. Microscopic examination unveils non-uniformity in the coating's distribution across the sheet. In addition, when the coated metal undergoes hot-pressing to fabricate individual parts, an IDL forms between the coating and base sheet metal, as shown

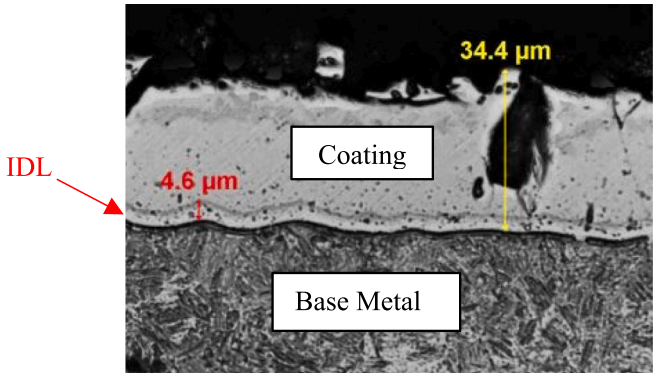

Fig. 4. Microscopy image of IDL in between base metal and coating.

on Fig. 4. The IDL is created when atoms from the base metal and coating material are energized and transition across to the other side, generating an additional metal alloy layer encompassing both the base metal and coating material. In the case of Al—Si coated metals, the IDL would be Fe—Al—Si [29]. This layer is formed somewhat unpredictably, owing to variations within the chemical composition of the coating and base material, alongside inconsistencies during the heating process. While the IDL forms somewhat consistently across an individual surface, the process uncertainties contribute to other sheets manifesting dissimilar IDL thicknesses, even with constant process parameters.

These inconsistencies introduce an uncertainty factor into the welding process, as IDL is not commonly measured on a large-scale production scale due to time and cost constraints. However, IDL wields substantial influence on welding quality. Notably, when analyzing the instances of expulsions observed during the welds conducted for this study, the IDL thickness exhibits the most distinct trend when compared to the other two input welding parameters (i.e., welding current and force), as illustrated in Fig. 5.

While larger welding currents and forces often correlates with a higher expulsion rate, a notable observation is that the presence of a larger IDL thickness almost guarantees expulsion, whereas an absence of IDL significantly raises the likelihood of expulsion. This underscores the critical role of IDL thickness knowledge for in-line decision-making processes. The most direct application is that the IDL information can enhance methods for detecting expulsions. Furthermore, it can facilitate proactive process adjustments in the welding production line. If IDL thickness is known prior to welding, the process parameters can be adjusted to configurations that would be less likely to expulse.

2.3. Proposed 4-Phase IDL-inclusive model

To account for the melting phase of the coating's IDL, a 4-Phase RSW model is proposed. Compared to Dickinson's 3-Phase model in Fig. 3, this 4-Phase model includes an additional IDL removal phase. Fig. 6 illustrate the changes of DR, electrode displacement (positive values indicating a widening between the electrodes and negative values indicating a contraction between the electrodes), and electrode force (the value of the force measured on the bottom electrode) during the 4 phases.

As previously stated, the initial drops in DR are not perceptible through indirect measurement of DR, so the first 2 phases in the Dickenson and other existing models are removed from discussion in this paper. In summary, the proposed RSW model comprises four primary phases: *material expansion*, *IDL removal*, *pre-molten joining*, and *nugget formation*. It's vital to note that while this model delineates distinct phases, these divisions solely highlight the prevailing mechanical aspect within each phase. In reality, mechanical phenomena overlap between phases, but the identification of dominant physics within each phase can provide valuable insights.

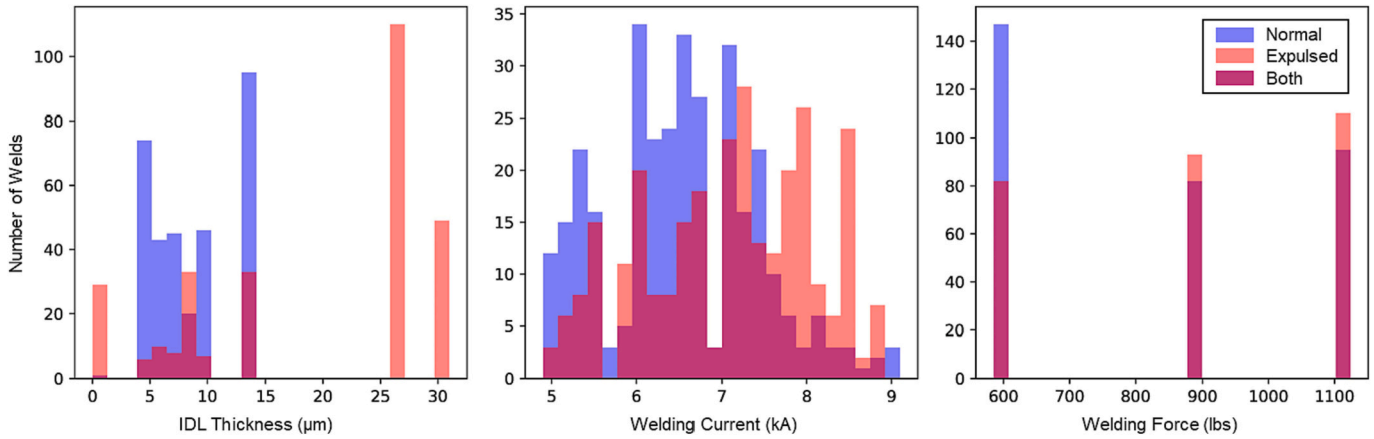

Fig. 5. Histograms of normal (blue) and expulsion (red) welds vs. IDL thickness, welding current, and force. Magenta colors represent the overlapping between normal and expulsed welds. (For interpretation of the references to color in this figure legend, the reader is referred to the web version of this article.)

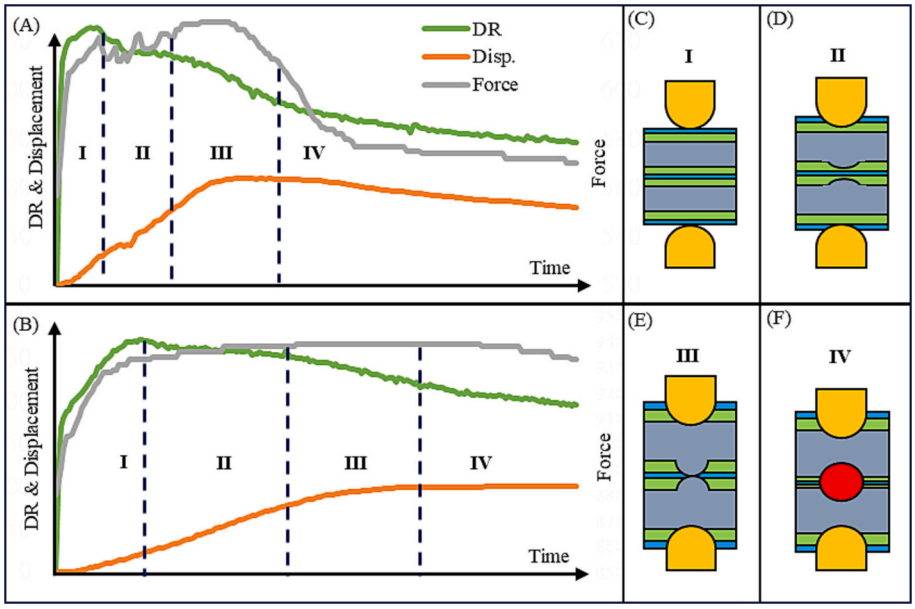

Fig. 6. The proposed 4-Phase IDL-inclusive model: (A) 4 phases for welding with IDL, (B) 4 phases for welding without IDL, (C)-(F): illustration of welding process during corresponding phases.

The expansion phase, as shown in Fig. 6C, aligns with conventional interpretation [6,7]. The DR curve shows constant growth attributed to rising temperature and increasing distance between electrodes. The displacement curve similarly rises, as a result of thermal expansion separating the electrodes. Also, no element within the stack-up yields to the force exerted by the electrodes, which induces a rise in the force, as the thermal expansion induces thermal strain that presses against the electrodes.

The IDL removal phase, as shown in Fig. 6D, shows distinct changes in the DR and force curve. Although continued thermal expansion and temperature elevation would typically cause an increase in resistivity, the IDL functions as a resistive element within the circuit. Consequently, its removal leads to an overall reduction in measured DR. The displacement curve continues its ascent, albeit with a change in concavity that signifies a deceleration in growth. This is because the base metal constituting the primary element of expansion continues to heat up and expand. The force undergoes a decline, usually followed by a phase of oscillations. This pattern emerges because the IDL is in effect expelled constantly, primarily from the surface, allowing it to burst radially from the electrode. It is important to note that despite these force drops, the overall expansion force is still higher than the clamping force. The expulsion of the IDL results in the loss of an expansion-contributing component, but the base metal continues to expand. This theory is supported by the observation related to welding metal without IDL in Fig. 6B. Although the changes in DR concavity can be observed and correlated with the proposed phases, the force drop, displacement rate shift, and substantial resistance drop are absent.

Subsequent to the removal of the IDL, the exposed metal interfaces directly with the electrodes and each other, as shown in Fig. 6E, in effect adhering to the uncoated model. In this phase, the metal experiences compression and shaping, effectively eliminating gaps and enlarging the conductive area. This counteracts the impacts of thermal expansion and the rising temperature. The displacement continues to rise, as the base metal comes into direct contact with the electrodes, asserting itself against the clamping force. This trend resonates within the force curve, which ascends and then stabilizes. This plateau emerges due to the temperature-induced reduction in the modulus of elasticity, and the expansive force approaches its threshold before the onset of melting.

Finally, the liquification of metal starts and the nugget begins to form, as shown in Fig. 6F. Although liquification and rising temperature

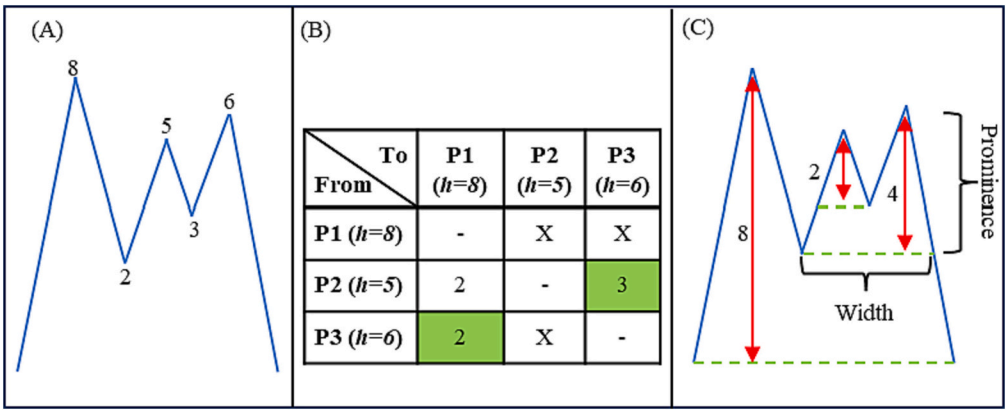

Fig. 7. Illustration of topographic prominence: (A) heights of peaks and valleys denoted in a time series; (B) pairing of peaks with numbers indicate the lowest value between the "To" and "From" peaks. X denotes that the "To" peak is not higher than the "From" peak. Highlighted cells denote the maximum value of that row; (C) the processed time series will all prominences denoted.

of the metal increase the resistance, the pores and gaps between the two sheets become filled, eliminating resistance-contributing elements. Additionally, material compression takes effect, leading to a further reduction in resistance. The liquification also allows expansion radially, away from the displacement and force measurements. This causes a continuous decrease in both measurements as the process comes to an end.

3. Feature extraction from the IDL-inclusive model

While conventional physical models primarily leverage DR peaks for quantifying weld quality and detecting defects, the proposed model facilitates the extraction of supplementary features, which more comprehensively unveil process dynamics, thereby augmenting quantitative modeling and prediction capabilities. This section introduces a systematic methodology that integrates data filtering, topographic prominence analysis, and logical rules to autonomously segment the phases. This allows a collection of meaningful features to be established from the four phases, with the intention of establishing correlations with IDL thickness.

3.1. Data filtering and phase determination

Moving RMS Filtering is commonly used in denoising RSW time series [17]. The number of neighbors used for this paper was chosen to be 2, creating a filtering window of 5. The selection of this particular value was a deliberate compromise aimed at eliminating subtle fluctuations while retaining more pronounced variations.

To detect the phase initiation times, a technique is needed to detect signal peaks, and topographic prominence is such a method. Based on geographic topography, this method can help differentiate noisy and steady data by attributing a prominence value influenced by neighboring data points [30]. Analogously, the prominence of a peak is the shortest vertical distance a hiker would need to travel to reach the base of a taller peak. The algorithm for finding the prominences goes as follows. First, all peaks in a time-series are identified. Then, each peak is paired with all other peaks that exceed it. Then the *minimum* value along the time-series between each pair is determined. The *maximum* of these values is the bottom of the peak's prominence. Extending the bottom of the prominence outward horizontally until it intersects with an edge determines its width. An example of this is shown on Fig. 7.

Drawing upon the fundamental physical mechanisms characterizing individual phases, a set of pivotal features emerges for potential application in the detection of phase transitions. Colloquially, the features are maximum resistance, force stabilization, and maximum displacement. Maximum resistance is a good indicator for transition from Phase 1 to Phase 2, as the initiation of IDL removal starts lowering the entire DR measurement. Force stabilization is particularly pronounced as the process transitions to Phase 3, as the temperature-induced reduction in the modulus of elasticity and the thermal expansion force approaches its plateau as the base metal has full contact with electrodes. Maximum displacement pinpoints the transition from Phase 3 to Phase 4, as the liquification and material compression make the electrode displacement continuously decrease. While maximum resistance and displacement are relatively straightforward to identify, the accurate detection of force stabilization is more challenging. This difficulty arises due to the inherent noise and oscillations within the force curve, attributed to the dynamic removal of IDL. Furthermore, the force curves exhibit diverse signal characteristics across different welding conditions, thereby amplifying the complexity of detecting force stabilization. In this paper, an innovative set of logical rules has been devised to robustly discern force stabilization and the onset of Phase 3. This approach has been tailored to accommodate diverse welding conditions and various force curve types, thus ensuring a dependable detection mechanism for force stabilization.

Force stabilization can be understood as the moment when the force starts to steadily rise and settles at a strong and stable level before metal liquefaction. In optimal situations, the force peak aligns with the force plateau situated midway through the welding process. Therefore, the fundamental criterion for identifying force stabilization involves locating the most prominent peaks of force curves. Due to the variability in force curves, the initial rule may not hold for all welding scenarios, so additional rules are needed. As the targeted plateau should exhibit a substantial and level profile, the RMS filtering is applied to smooth raw force curves. In addition, all values are truncated to integers, facilitating

Table 1
Logical rules for identifying force stabilization under different welding situations. Dotted red line is the registered dominant peak and solid blue line is the peak as identified force stabilization.

Welding situation	Force curve	Logical rules
Force spike before stabilization	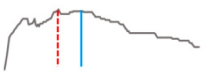	RMS smoothing with integer truncation
Large spike before IDL removal	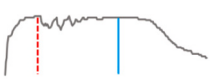	Ignore first peak
Stabilization after expulsion	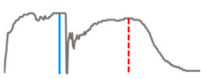	Only consider peaks before max. Displacement

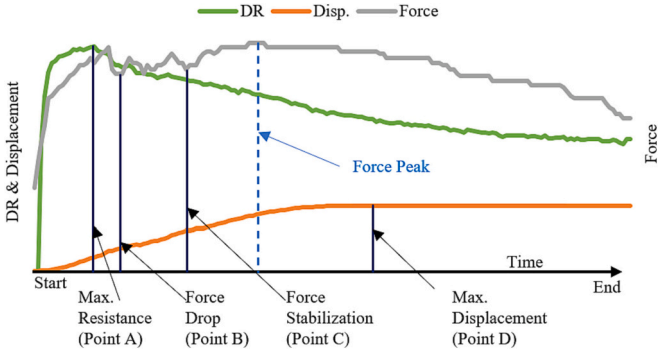

Fig. 8. Typical weld with marked extracted features and the force peak.

the elimination of minor irregularities that could trigger false peak detection. Then all peaks within the filtered time series are found through topographic prominence. To mitigate the impact of process noise, peaks of a prominence value 1 are ignored. There are instances where the initial force peak, indicating the culmination of thermal expansion, may register as overly elevated and dominant. Hence, the first force peak is excluded. Conversely, expulsion can cause chaotic disruptions during the liquification phase that can also register as the dominant peak. Consequently, any peaks emerging after the maximum displacement, indicative of the commencement of phase 4, are further excluded. These situations and logical rules for accurate identification of force peak and stabilization are summarized in Table 1.

3.2. Feature extraction

Though these phase transition-related features encompass a wide spectrum of process mechanics, they do not inherently establish a direct correlation to the IDL removal: the peak resistance occurs prior to IDL liquification while the force stabilization is after IDL removal. Introducing a feature that corresponds to this particular event enhances the comprehensive depiction of the IDL removal process. For the sake of simplicity in explanation and broad applicability across different weld scenarios, a novel feature has been incorporated into the transition features. This feature, informally denoted as a "Force Drop," pertains to the time during this phase when the force reaches its lowest value.

For brevity, the key feature times, revealed by the maximum resistance, force drop, force stabilization, and maximum displacement, are referred to points A, B, C, and D, respectively, as shown in Fig. 8. For each point, the time and values of each of the measured curves (i.e., DR, force, displacement) are defined as process features. Additionally, value changes and rate of changes (RoC) between consecutive points are also included as process features, alongside the starting and ending values of each measured curve. In the rare case where there is no detected force stabilization (likely associated with welding without IDL), all singular features related to Point C are ignored.

To assess the influence of incorporating these diverse features on predicting IDL thickness, 4 different feature sets are defined and compared. The first set uses only point A, maximum resistance, as it is the most common feature in RSW time series analysis. The second set adds Point D, maximum displacement, since this is a feature that is easy to extract, explain, and occurs the farthest away from Point A. The third set adds point C, force stabilization, which makes this set consist entirely of the phase transition information. Finally, the fourth set uses all the extracted features as previously discussed. The feature sets are summarized in Table 2.

4. Data-driven correlation from physical features to IDL thickness prediction

While physical models offer valuable insights into process dynamics and enable the extraction of features for process characterization, they lack the capacity for quantitative process modeling and prediction of relevant variables (such as IDL thickness and expulsion in this study). In contrast, data-driven Machine Learning (ML) techniques are better suited for this purpose, as they quantitatively model the relationships between meaningful physical features and variables of interest. In this paper, a straightforward neural network architecture known as a Multilayer Perceptron (MLP) [31], is investigated, motivated by the MLP's lower computational complexity and improved model generalizability compared to more advanced ML techniques.

MLPs represent one of the earliest and extensively employed Neural Network (NN) structures for establishing connections between discrete inputs and outputs. The advantage of MLPs lies in their ability to capture intricate, interlinked, and non-linear relationships using interconnected "neurons" and activation functions. The neurons are stacked in hidden layers between the input and outputs of the network. The number of hidden layers and the number of neurons within those layers affect the capacity of the network. The activation functions give the MLP non-linearity. Common functions are Rectified Linear Unit (ReLU), sigmoid, and hyperbolic tangent. The MLP model of a 3-layer (i.e., 1 input layer, 1 hidden layer, and 1 output layer) perceptron can be expressed as:

$$\mathbf{y} = f(W_2 * f(W_1 \mathbf{x})) \tag{1}$$

Similar to the training in other ML techniques, the essence of the MLP's training is imparting the network with learning from labeled data. This is handled through the application of a loss function, which

Table 2
Summary of all features extracted from the process measurement.

Feature Sets:	1	2	3	4
Time of:	A	A	A	A
Value of Resistance at Time:			C	B
Value of Force at Time:		D	D	C
Value of Displacement at Time:				D
Resistance Difference:	Start→A	Start→A	Start→A	Start→A
Resistance RoC of:	A→End	A→D	A→C	A→B
Force Difference of:		D→End	C→D	B→C
Force RoC of:			D→End	C→D
Displacement Difference of:				D→End
Displacement RoC of:				

Table 3
Details of all welding trials performed in the experimental study.

Force (lbs)	Time (ms)	Thickness (mm)	IDL (μm)	Current (kA)
585	170	1	4	4.9, 5, 5.2(×3), 5.4(×4), 5.6, 6 (×2), 6.2, 6.4, 6.6, 6.8, 7(×2), 7.2–8.8 (0.2 inc), 9.1
			7	5–7.2 (0.2 inc), 6.65, 7.5, 5.1, 5.4
			13	5, 5.2, 5.4(×2), 5.5, 5.6, 5.8(×2), 6(×4), 6.2, 6.3, 6.4, 6.6, 6.9
			31	5, 5.2, 5.4(×2), 5.5, 5.6(×3), 5.8 (×3), 6(×4), 6.2, 6.5
899	200	1.4	0	5, 6.2, 6.4, 6.6, 6.7, 6.8, 7(×3), 7.2 (×4), 7.4, 7.7
			10	6, 6.1, 6.2, 6.4(×3), 6.6(×4), 6.8, 7, 7.2, 7.4, 7.5, 7.6, 7.8, 8, 8.3
			13	5.7, 6(×2), 6.2(×4), 6.6, 6.65, 6.8 (×2), 7, 7.3
			26	6, 6.2, 6.6, 6.7, 6.8(×2), 7(×4), 7.2(×4), 7.4, 7.7
1124	240	1.8	6	6–6.8(0.2 inc), 6.9, 7(×2), 7.2 (×2), 7.4(×4), 7.6, 7.7, 7.8, 8, 8.3
			8	6.6–7.4(0.2 inc), 7.6(×2), 7.8, 7.9, 8(×2), 8.2(×2), 8.4(×4), 8.6, 8.9
			13	6.5, 6.6, 6.8(×2), 7(×4), 7.2, 7.4, 7.6, 7.8, 8, 8.3
			27	6.6, 6.8, 7, 7.2, 7.4, 7.6(×2), 7.8 (×3), 7.9, 8(×), 8.2(×2), 8.4(×4), 8.6, 8.9

quantitatively evaluates the network's performance by comparing the network's predictions to the ground truth values, colloquially known as prediction error. In regression problems, Mean Squared Error (MSE) loss is commonly used, whereas Cross Entropy (CE) loss is common for classification problems [32]. In this way, training can be viewed as an iterative optimization problem that determines what network weights minimize the prediction error. This optimization problem is achieved through determining the gradient of the network, which can be numerically approximated by calculating the gradient of loss function with respect to network weights through backpropagating the network using a chain rule. The network gradients allow the weights to be updated through gradient descent [33]:

$$W_i^{(n+1)} = W_i^{(n)} - \alpha \times \partial L \Big/ \partial \mathrm{W}_i^{(n)} \tag{2}$$

A common issue in ML is the phenomenon of overfitting, where a model over fits its predictions to the training data, at the cost of adaptability to other data. Metaphorically, the model "memorizes" solutions based on the training data, yet lacks the ability to "reason" accurate outcomes for unseen data. To mitigate this issue, dropout layers are implemented. During training, each neuron is assigned a predefined probability of "dropping out," rendering it inactive in shaping the final prediction. This allows more nuanced features to not be outweighed by more impactful ones and improves the model's generalizability [34].

In this study, the network is structured as a 4-layer MLP: 1 input layer with the number of input neurons equal to the number of physical features (as defined in Table 2), 2 hidden layers encompass a number of hidden neurons equivalent to twice the number of input neurons, and 1 output layer with one output neuron. This way of configuring hidden layers is to accommodate varying input sizes, mitigating the risk of overfitting for smaller feature sets or underperformance for larger ones. The two hidden layers are augmented with a 0.3 dropout rate and employ the ReLU activation function. MSE is used as the loss function for IDL prediction and Binary Cross Entropy is used for the expulsion classification. The Adam optimizer is used to train the network with a learning rate of 0.0001.

Table 4
Number of input features considering different categorizations of measurements and features.

Process measurement set	Feature set (defined in Table 2)			
	1	2	3	4
DR	8	12	16	20
DR & F	13	20	27	34
DR, F, & disp.	18	28	38	48

5. Experimental setup and data collection

To validate the proposed IDL-inclusive physical model and evaluate the efficacy of features extracted from this model in predicting IDL thickness and detecting expulsions in a quantitative manner, a comprehensive series of RSW experiments were conducted. These experiments encompassed hundreds of RSW welds executed under diverse welding conditions. The corresponding process measurement data, including DR, electrode force, and displacement, were meticulously recorded and collected for analysis.

The welds were manually performed using a Milco RSW gun driven by a WTC medium frequency controller, which measured the secondary welding current. The electrodes were C15000 CuZr button caps with a face diameter of 6 mm. A Kistler strain gauge with 2 % error precision was mounted on the lower electrode arm to measure the electrode force. A Heidenhain linear encoder with an accuracy of ±5 μm was mounted on the lower electrode arm to measure the electrode displacement. The sheet metal used was Usibor® 1500, which had been coated with a 40-μm layer of Aluminum Silicone. The experiments were performed under 3 unique sets of sheet thickness, welding force, and time, as shown in Table 3. The welding forces used were 585 lbs, 899 lbs, and 1124 lbs with welding times of 170 ms, 200 ms, and 240 ms. The sheet thicknesses (t) used were 1, 1.4, and 1.8 mm. These sheets were further differentiated by sorting them based on their measured IDL thickness. These sheets were then welded under varying currents, as detailed in Table 3. The initial configuration involved aligning two sheets to create a stack-up. Subsequently, three spot welds were executed, commencing from the center and progressing to one on each side of the initial weld. A total number of 627 welds were collected. Throughout the welding process, if any noticeable expulsion occurred and was observed, the respective weld was designated as having experienced expulsion. Electrodes were dressed between each trial.

For each experiment, features were automatically extracted from process measurements in the way described in Section 3.2. To evaluate the significance of the supplementary insights gained from distinct process measurements, the data was categorized into measurement subsets. The first set includes only the DR measurement, the second incorporates the force (F) measurement, and the final set adds displacement (Disp.) measurement. This categorization was paired with the feature sets described in Section 3.2 to create 12 different sets of input features to be used in the MLP for IDL thickness prediction. It should be noted that welding current and force are included in all sets of input features. The total numbers of input features for the 12 sets are shown in Table 4.

To validate the hypothesis that IDL thickness significantly influences the probability of expulsion, three distinct input sets are assessed in conjunction with a binary classifier trained to forecast expulsion occurrences. The initial input set comprises solely of the input current and force. The second input set incorporates the input current, force, and the measured (ground truth) IDL thickness. Finally, the third input set integrates the input current, force, and the predicted IDL thickness as determined by the previously discussed trained MLP. The first set establishes a baseline, and any enhancements by the other two sets in predictive accuracy would predominantly emphasize the critical role of IDL in impacting process stability and expulsion.

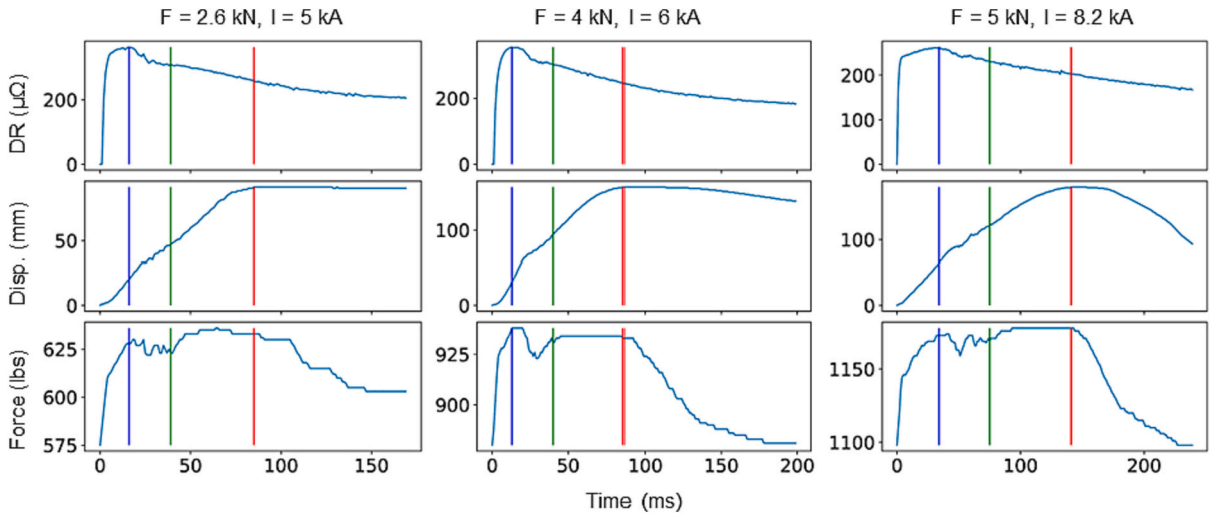

Fig. 9. Detected phase transition points for welds under three different welding parameters. Blue line represents maximum resistance, green line is force stabilization, and red line is maximum displacement. (For interpretation of the references to color in this figure legend, the reader is referred to the web version of this article.)

6. Results and discussions

The session will evaluate the performance and robustness of the developed method for automatic detection of the proposed 4 phases, when handling various welding scenarios. Then, the results of IDL thickness prediction based on features derived from the IDL-inclusive 4-phase model and quantitative MLP modeling are presented. Last, discussions on the influence of IDL on expulsion occurrences are expanded.

6.1. Automatic phase detection

The developed automatic phase detection method, a systematic solution of data filtering, topographic prominence, and logical rules, are in general able to accurately identification the key phase transition points in most welding scenarios. Examples of the method's performance in processing normal welds are shown on Fig. 9.

While the second and third phase transition points accurately reflect the transitions from IDL removal to pre-molten joining and nugget formation, the first detected phase transition point (maximum resistance) does not truly reflect the end of thermal expansion. As can be seen in Fig. 10, the detected phase transition point occurs slightly before the true end of the thermal expansion phase.

The actual shift from Phase 1 to 2 is represented by a change in the curvature of the displacement curve and a decline in the force curve, when the metal starts undergoing partial plastic deformation. This phenomenon is discernible from the force curve displaying a slight leveling, indicating a deceleration in the expansion force. The automatic identification of this phase transition would commence by searching for the initial decrease in force following the peak resistance point. However, this process would necessitate additional fuzzy logical rules, introducing more computational complexity and uncertainty. Considering a trade-off between phase detection accuracy and computational complexity, peak resistance is an intuitive and ideal feature than can generally capture the transition from thermal expansion phase to IDL removal phase.

The transition point from Phase 2 to Phase 3, force stabilization as explained in Section 3.1, needed additional logical rules to handle various welding scenarios. Overall, this goal is accomplished, with examples related to welding scenarios listed in Table 1 shown in Fig. 11.

The developed phase transition detection method can possibly fail under expulsion cases, where the maximum displacement occurs after the expulsion occurrence, as illustrated in Fig. 12 that shows two expulsed welds with no IDL. In the left weld, the detected phase transition points accurately matched the anticipated points in time. As there is no IDL to remove, the shift from Phase 1 to 2 (green line) is set at time 0, according to the logical rules developed in Section 3.1. Conversely, in the right weld, a wrong shift from Phase 1 to 2 is labeled. This misdetection is caused by the maximum displacement occurring after an expulsion. This welding scenario is somewhat uncommon, and it happens if a minor expulsion occurs early in the process. In normal welds, the maximum displacement occurs when liquid dynamics become the dominant factor in the process, and expulsions typically occur at or after that moment. In this way, the red line should ideally be just behind the first expulsion, which would also stop the detection of force stabilization, bringing it in line with the left weld. While this could be likely done by adding more logical rules, the additional rules may open more room for detection exceptions and mistakes. Consequently, due to the potential risk of disrupting the phase detection in the majority of welding scenarios, the precise identification of this infrequent welding case is not pursued.

6.2. IDL thickness prediction

IDL thickness is predicted using the different sets of features extracted from the IDL-inclusive physical model through MLP-based modeling. The performance of IDL thickness prediction is shown in Table 5, evaluated in the coefficient of determination (R^2) by comparing the predicted to true thickness. Predictions pertaining to different feature sets (noted as FS, defined in Table 2) and process measurement sets (noted as PMS, defined in Table 4) are also compared in Table 5. Among the 627 welds, an 80/20 split ratio was used in creating training and validation data subsets. The validation results shown in Table 5 are generated through 5-fold validation for individual combinations of measurement sets and feature sets. These combinations were tested 4 times, a total of 20 training cycles, to mitigate randomness in the performance. The mean and standard deviation of these 20 cycles are presented.

Regarding the PMS, it's evident that the inclusion of displacement measurement contributes a substantial amount of information for improved IDL prediction. This is evident from the consistent performance across all four FS when displacement data is included, in contrast to the more diverse outcomes observed with other PMS. This outcome is logical, given that displacement measurement directly reflects part thickness, which as previously mentioned is notably influenced by the initial thickness of the material stack-up. These results also highlight the significance of the features derived from the IDL-inclusive 4-phase

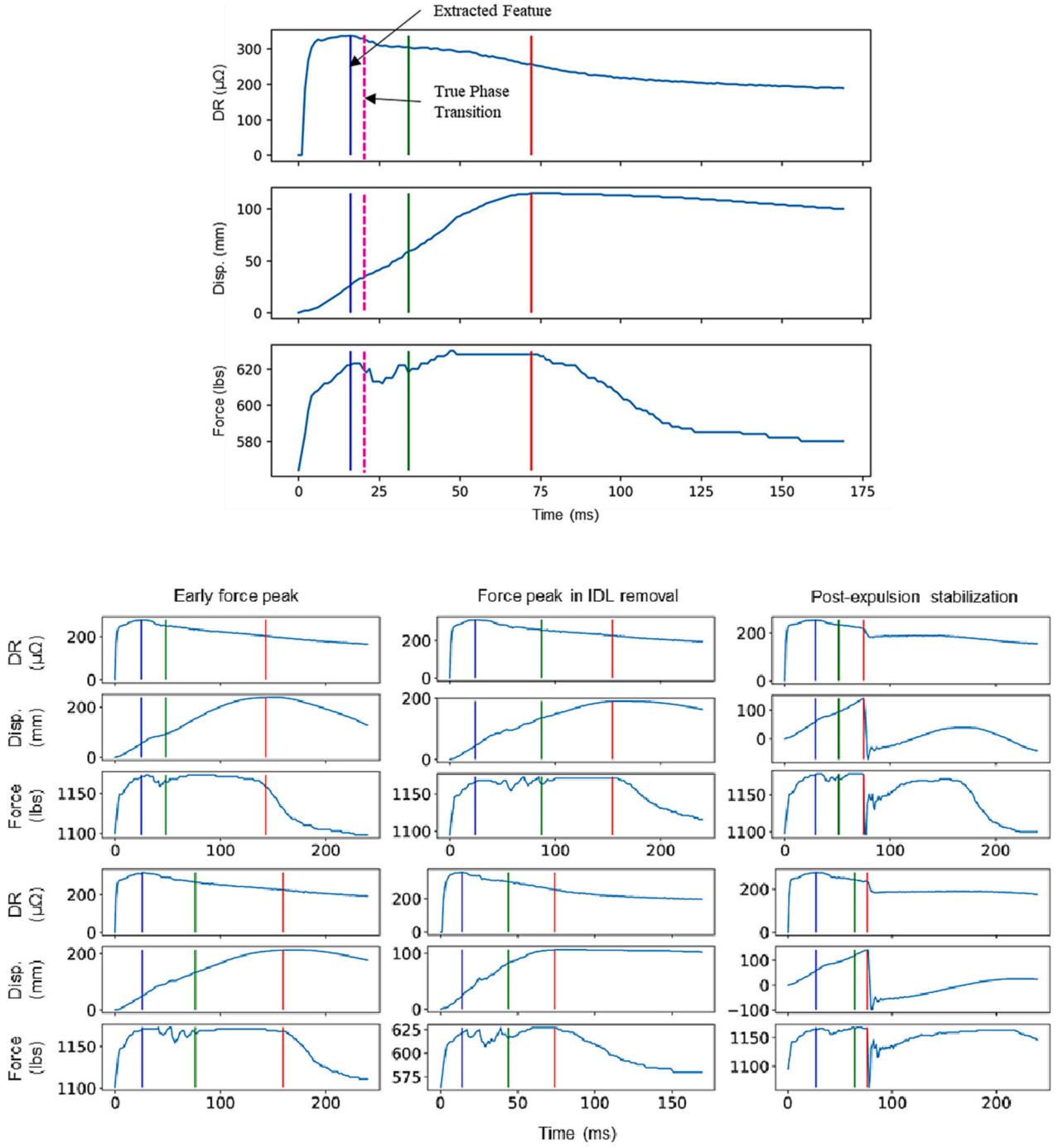

Fig. 10. Detected phase transition points and true transition from Phase 1 to 2 (dotted magenta line). (For interpretation of the references to color in this figure legend, the reader is referred to the web version of this article.)

model. Specifically, all experiments employing FS 3 (derived upon force stabilization) and FS 4 (derived upon force drop) attained R^2 values exceeding 0.9. The inclusion of the force drop shows the more significant performance increase. This is attributed to the fact that force drop directly measures the removal of the IDL, in contrast to other features that capture aspects before or after the IDL removal in the process.

The plots of predicted vs. true IDL thickness for using only DR measurement (i.e., the first row of Table 5) are shown in Fig. 13. Simply comparing the R^2 indicates that inclusion of more physical features reveals more information of the process dynamics and hence improves the prediction performance.

Upon observing the prediction versus true graphs, it became evident that all networks exhibited similar performance for low IDL thicknesses. However, certain problematic welds introduced bias to the results. Notably, these issues were prominent in the 13-μm IDL thickness range, where the networks tended to overestimate, and in the 26 to 31-μm range, where the networks tended to underestimate. This discrepancy is primarily attributed to the networks estimating values around the mean of the available data. Importantly, the lack of welds with IDL thicknesses falling between 13 and 26 μm compelled the networks to conjecture about such values rather than relying on learned patterns. The efficacy of the networks hinges on how they handle these unusual welds. Less proficient networks distributed their predictions more broadly, whereas more adept networks clustered their predictions around the actual

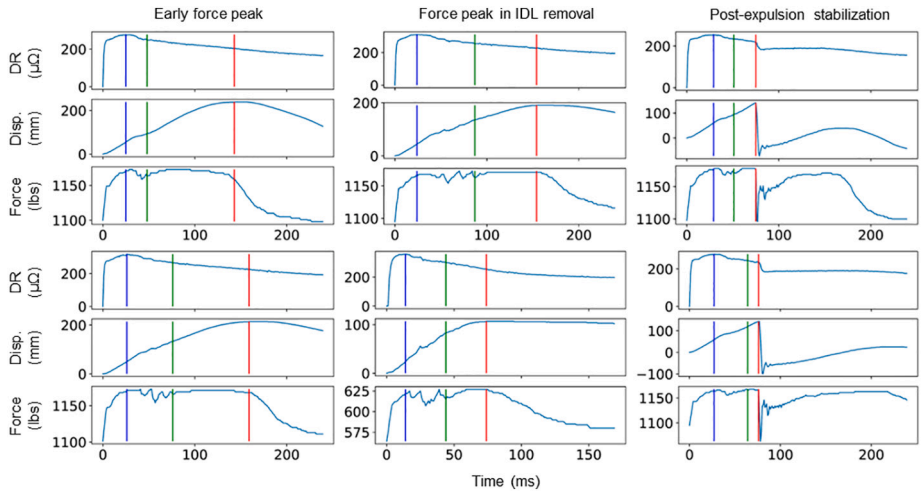

Fig. 11. Phase detection results for various welding scenarios listed in Table 1.

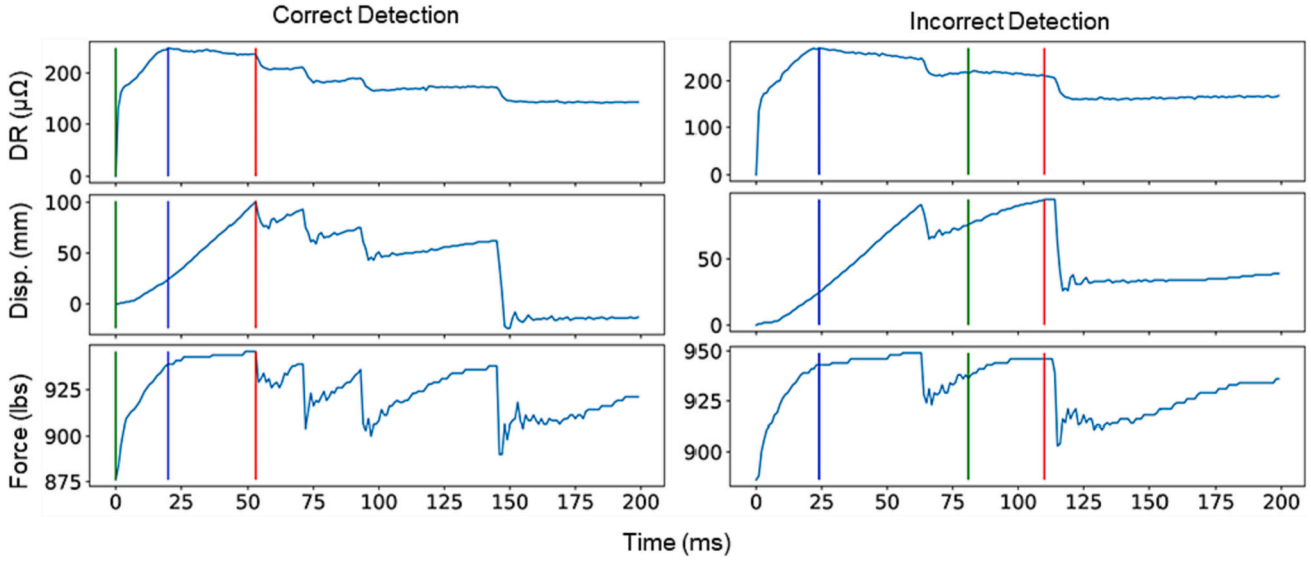

Fig. 12. Phase transition detection of expulsed weld with no IDL.

Table 5
IDL thickness prediction using different feature sets (FS) and process measurement sets (PMS). Performances are evaluated in R^2 and 5-fold validation. The best performance for each PMS is highlighted in bold.

FSPMS	Training				Validation			
	1	2	3	4	1	2	3	4
DR	0.782 ± 0.037	0.869 ± 0.023	0.901 ± 0.028	**0.939 ± 0.014**	0.849 ± 0.019	0.890 ± 0.024	0.909 ± 0.029	**0.943 ± 0.018**
DR & F	0.875 ± 0.025	0.925 ± 0.020	0.951 ± 0.012	**0.974 ± 0.003**	0.902 ± 0.034	0.916 ± 0.023	0.926 ± 0.029	**0.948 ± 0.024**
DR, F, & disp.	0.939 ± 0.010	0.964 ± 0.011	0.972 ± 0.017	**0.981 ± 0.005**	0.940 ± 0.036	0.947 ± 0.015	0.957 ± 0.015	**0.965 ± 0.013**

value, despite some predictions being significantly inaccurate. Incorporating additional process-related information does have the potential to mitigate this problem, as evidenced by the comparison between the results of FS 4 and FS 1, where the predictions become more clustered for the same IDL thickness. However, a more foundational solution would involve collecting more data that covers the range of missing IDL thicknesses.

6.3. Expulsion detection upon inclusion of IDL

As anticipated in Section 2.3, it was hypothesized that IDL thickness significantly influences the occurrence of expulsions. However, this relationship is not linear, as indicated by the non-linear pattern in Fig. 5. By quantifying the complex interplay between expulsion occurrence, IDL thickness, and welding process parameters (such as welding current and force) through data-driven modeling, it becomes feasible to utilize a few sample welds from a new batch of sheet metals to accurately predict the likelihood of expulsions under various process conditions. This predictive capability can then be harnessed to optimize the welding process settings for that specific batch of material, ultimately reducing the occurrence of expulsions. In this study, the expulsions in welds are classified using three different input combinations: process settings only,

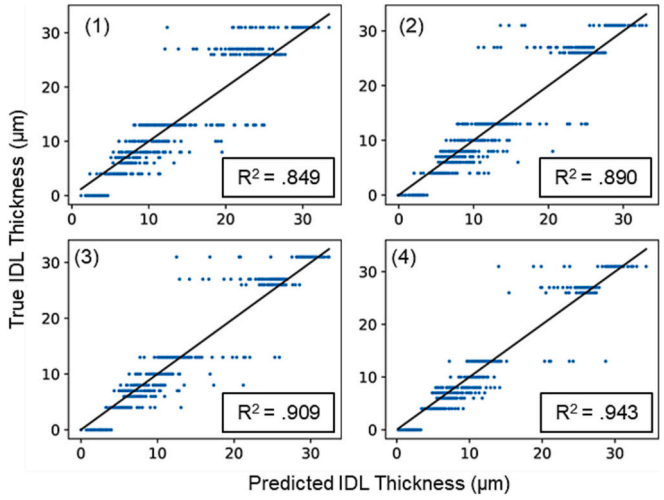

Fig. 13. Predicted vs. true IDL thickness when only DR measurement is applied. (1)–(4) represent 4 feature sets, defined in Table 2.

Table 6
Training and validation performance of MLP-based expulsion classification, with different sets of inputs. Results come out of a 5-fold validation.

Inputs	Current & force	Current, force, & true IDL thickness	Current, force, & predicted IDL thickness
Training accuracy	0.589 ± 0.044	0.754 ± 0.071	**0.767 ± 0.055**
Validation accuracy	0.699 ± 0.072	**0.838 ± 0.040**	0.835 ± 0.035
Validation precision	0.715 ± 0.184	**0.917 ± 0.035**	0.916 ± 0.047
Validation recall	0.588 ± 0.154	**0.842 ± 0.045**	0.819 ± 0.094
Validation F1	0.642 ± 0.160	**0.877 ± 0.034**	0.862 ± 0.066

process settings combined with ground truth IDL thickness, and process settings combined with predicted IDL thickness obtained using the methodology outlined in Section 6.2. The latter two combinations are compared to assess the equivalence of information between predicted and true IDL thickness, as well as the effectiveness of predicted IDL thickness in predicting expulsion likelihood. These models were trained with the same training/validation split of the 627 welds with 5-fold validation 4 times to mitigate randomness. The results of the expulsion classification using these three input combinations are presented in Table 6.

The inclusion of both the true and predicted IDL thickness yields a notable enhancement in the networks' capability to forecast expulsions, resulting in a substantial 13 % increase in classification accuracy. It is intriguing to note that the network utilizing the predicted IDL thickness performs only slightly inferior to the network using the true IDL thickness. This suggests that even a rough estimate of the IDL thickness can furnish valuable insights for predicting the occurrence of expulsions.

Observing the confusion matrices, as depicted in Fig. 14, reveals that all networks tend to generate false positives, where normal welds are identified as expulsed welds. This could be attributed to the fact that expulsed welds can transpire in process settings where normal welds are also formed, as illustrated by the overlapping distributions between normal and expulsed welds in Fig. 5. Without supplementary information, such as in-situ measurements, the networks could become perplexed. Additionally, it's noteworthy that predictions based on both true and predicted IDL have significantly diminish false negatives, where expulsed welds are identified as normal welds. This suggests that incorporating IDL can substantially enhance the performance of identifying problematic welds. This aligns with the assertion made in section 2.3, highlighting the strong role of IDL thickness as an indicator for the likelihood of expulsion.

7. Conclusions

In this paper, an IDL-inclusive 4-phase physical RSW model is introduced. Compared to existing RSW models, the proposed model accounts for the unique phase and phenomena related to the IDL layer, which is crucial for predicting both IDL thickness and the likelihood of expulsion. Together, the redefined 4 phases of the RSW process are material expansion, IDL removal, pre-molten joining, and nugget formation. To automatically detect phase transitions based on in-situ process sensing (i.e., DR, electrode force, and displacement), a systematic approach that combines data filtering, topographic prominence, and logical rules is developed. Subsequently, features related to key phase transition points are defined and extracted from the process sensing, and are then quantitatively correlated with IDL thickness and expulsion occurrences through an MLP to create an interpretable data-driven model for process prediction. The importance and practicality of these features, particularly the force drop feature associated with the suggested IDL removal phase, are confirmed by the improved prediction performance. The impact of IDL thickness on expulsion likelihood is hypothesized, demonstrated by an improvement in expulsion detection accuracy from 70 % to 84 %. By further looking into the expulsion detection accuracies, it's found that utilizing process settings and IDL thickness predictions can significantly decrease the occurrence of false positive classifications in expulsion prediction, from over 26 % to below 7 %.

The success of the prediction networks for IDL thickness and expulsion demonstrates the feasibility of an explainable in-line monitoring system for detecting sheet metal stack-ups prone to expulsion. By knowing the IDL ahead of time or estimating it from a few sample welds

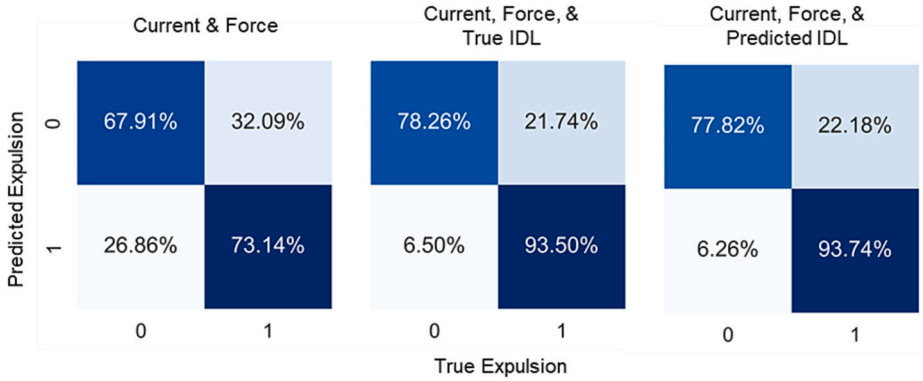

Fig. 14. Predicted vs. true expulsion confusion matrices for all input combinations: 0 represents normal welds and 1 represents expulsed welds.

in a new batch of sheet metals, expulsion likelihood can be predicted under various process conditions for that specific material batch. These predictions can guide the optimization of welding process settings to minimize problematic welds.

It is important to underscore that phase transitions can be identified using all three process measurements (DR, force, and displacement), which simplifies data processing and feature extraction. However, due to limited sensing capabilities in many existing welding plants, often only DR can be measured. To enhance the practical applicability of these methods, future work will focus on developing a methodology to detect phase transitions and extract characteristic features solely using the DR measurement.

Declaration of competing interest

The authors declare that they have no known competing financial interests or personal relationships that could have appeared to influence the work reported in this paper.

Acknowledgements

This paper is based upon work supported by the National Science Foundation under Grant No. 2237242.

References

[1] Ma Y, Wu P, Xuan C, Zhang Y, Su H. Review on techniques for on-line monitoring of resistance spot welding process. Adv Mater Sci Eng 2013;2013:1–6. https://doi.org/10.1155/2013/630984.
[2] Wang Y, Rao Z, Wang F. Heat evolution and nugget formation of resistance spot welding under multi-pulsed current waveforms. Int J Adv Manuf Technol 2020;111(11−12):3583–95. https://doi.org/10.1007/s00170-020-06337-z.
[3] Ao S, Li C, Huang Y, Luo Z. Determination of residual stress in resistance spot-welded joint by a novel X-ray diffraction. Measurement 2020;161:107892. https://doi.org/10.1016/j.measurement.2020.107892.
[4] Richard AA, Traub AC, Vanzetti R. Real-time control of nugget formation in spot welds. Euromicro Newslett 1980;6(5):296–303. https://doi.org/10.1016/0303-1268(80)90163-7.
[5] Summerville, C., Adams, D., Compston, P., & Doolan, M. (2017). Nugget diameter in resistance spot welding: a comparison between a dynamic resistance based approach and ultrasound C-scan. Proc Eng, 183, 257–263. doi:https://doi.org/10.1016/j.proeng.2017.04.033.
[6] Dickinson DW, Franklin JE, Stanya A. Characterization of spot welding behavior by dynamic electrical parameter monitoring. Weld J 1980;59(6):170.
[7] Batista M, Furlanetto V, Duarte Brandi S. Analysis of the behavior of dynamic resistance, electrical energy and force between the electrodes in resistance spot welding using additive manufacturing. Metals 2020;10(5):690. https://doi.org/10.3390/met10050690.
[8] Williams NT, Parker JD. Review of resistance spot welding of steel sheets part 1 modelling and control of weld nugget formation. Int Mater Rev 2004;49(2):45–75. https://doi.org/10.1179/095066004225010523.
[9] Xia Y-J, Lv T-L, Li Y-B, Ghassemi-Armaki H, Carlson BE. Quantitative interpretation of dynamic resistance signal in resistance spot welding. Weld J 2023;102(4):69–87. https://doi.org/10.29391/2023.102.006.
[10] Andronie M, Lăzăroiu G, Ștefănescu R, Uță C, Dijmărescu I. Sustainable, smart, and sensing technologies for cyber-physical manufacturing systems: a systematic literature review. Sustainability 2021;13(10):5495. https://doi.org/10.3390/su13105495.
[11] Erol S, Schumacher A, Sihn W. Strategic guidance towards industry 4.0 — a three-stage process model. Int Conf Compet Manuf 2016;9(1):495–501.
[12] Wang SC, Wei PS. Modeling dynamic electrical resistance during resistance spot welding. J Heat Transfer 2000;123(3):576–85. https://doi.org/10.1115/1.1370502.
[13] Wang X-J, Zhou J-H, Yan H-C, Pang CK. Quality monitoring of spot welding with advanced signal processing and data-driven techniques. Trans Inst Measure Cont 2017;40(7):2291–302. https://doi.org/10.1177/0142331217700703.
[14] Hwang I, Yun H, Yoon J, Kang M, Kim D, Kim Y-M. Prediction of resistance spot weld quality of 780 MPa grade steel using adaptive resonance theory artificial neural networks. Metals 2018;8(6):453. https://doi.org/10.3390/met8060453.
[15] Russell M, Kershaw J, Xia Y, Lv T, Li Y, Ghassemi-Armaki H, et al. Comparison and explanation of data-driven modeling for weld quality prediction in resistance spot welding. J Intell Manuf 2023. https://doi.org/10.1007/s10845-023-02108-1.
[16] Ding H, Gao RX, Isaksson AJ, Landers RG, Parisini T, Yuan Y. State of AI-based monitoring in smart manufacturing and introduction to focused section. IEEE/ASME Trans Mechatron 2020;25(5):2143–54. https://doi.org/10.1109/tmech.2020.3022983.
[17] Zaharuddin MF, Kim D, Rhee S. An ANFIS based approach for predicting the weld strength of resistance spot welding in artificial intelligence development. J Mech Sci Technol 2017;31(11):5467–76. https://doi.org/10.1007/s12206-017-1041-0.
[18] Zhou B, Pychynski T, Reischl M, Kharlamov E, Mikut R. Machine learning with domain knowledge for predictive quality monitoring in resistance spot welding. J Intell Manuf 2022;33:1139–63. https://doi.org/10.1007/s10845-021-01892-y.
[19] Xing B, Xiao Y, Qin QH, Cui H. Quality assessment of resistance spot welding process based on dynamic resistance signal and random forest based. Int J Adv Manuf Technol 2017;94(1–4):327–39. https://doi.org/10.1007/s00170-017-0889-6.
[20] Lee J, Noh I, Jeong SI, Lee Y, Lee SW. Development of real-time diagnosis framework for angular misalignment of robot spot-welding system based on machine learning. Proc Manuf 2020;48:1009–19. https://doi.org/10.1016/j.promfg.2020.05.140.
[21] El-Sari B, Biegler M, Rethmeier M. Investigation of the extrapolation capability of an artificial neural network algorithm in combination with process signals in resistance spot welding of advanced high-strength steels. Metals 2021;11(11):1874. https://doi.org/10.3390/met11111874.
[22] Panza L, De Maddis M, Spena PR. Use of electrode displacement signals for electrode degradation assessment in resistance spot welding. J Manuf Process 2022;76:93–105. https://doi.org/10.1016/j.jmapro.2022.01.060.
[23] Ulaby FT, Maharbiz MM. Circuits. National Technology & Science Press; 2013.
[24] Silber RE, Secco RA, Yong W, Littleton JA. Electrical resistivity of liquid Fe to 12 GPa: implications for heat flow in cores of terrestrial bodies. Sci Rep 2018;8(1). https://doi.org/10.1038/s41598-018-28921-w.
[25] Goodno BJ, Gere JM. Mechanics of materials. Cengage Learning; 2009.
[26] Yakout M, Elbestawi MA, Veldhuis SC. A study of thermal expansion coefficients and microstructure during selective laser melting of Invar 36 and stainless steel 316L. Addit Manuf 2018;24:405–18. https://doi.org/10.1016/j.addma.2018.09.035.
[27] Wang W, Liu B, Kodur V. Effect of temperature on strength and elastic modulus of high-strength steel. J Mater Civil Eng 2013;25(2):174–82. https://doi.org/10.1061/(asce)mt.1943-5533.0000600.
[28] Li YB, Lin ZQ, Hu SJ, Chen GL. Numerical analysis of magnetic fluid dynamics behaviors during resistance spot welding. J Appl Phys 2007;101(5):053506. https://doi.org/10.1063/1.2472279.
[29] Liang W, Tao W, Zhu B, Zhang Y. Influence of heating parameters on properties of the Al-Si coating applied to hot stamping. Sci China Technol Sci 2017;60(7):1088–102. https://doi.org/10.1007/s11431-016-0231-y.
[30] Llobera M. Building past landscape perception with GIS: understanding topographic prominence. J Archaeol Sci 2001;28(9):1005–14. https://doi.org/10.1006/jasc.2001.0720.
[31] Murtagh F. Multilayer perceptrons for classification and regression. Neurocomputing 1991;2(5–6):183–97. https://doi.org/10.1016/0925-2312(91)90023-5.
[32] Golik, P., Doetsch, P., & Ney, H. (2013). Cross-entropy vs. squared error training: a theoretical and experimental comparison. Interspeech 2013. Doi:10.21437/interspeech.2013-436.
[33] Kingma DP, Ba J. Adam: a method for stochastic optimization. arXiv 2014. preprint, arXiv:1412.6980.
[34] Srivastava N, Hinton G, Krizhevsky A, Sutskever I, Salakhutdinov R. Dropout: a simple way to prevent neural networks from overfitting. J Mach Learn Res 2014;15(1):1929–58.